Progesterone receptor isoform B regulates the *Oxtr-Plcl2-Trpc3* pathway to suppress uterine contractility

Mary C. Peavey[a,1], San-Pin Wu[b,1], Rong Li[b], Jian Liu[b], Olivia M. Emery[b], Tianyuan Wang[c], Lecong Zhou[c], Margeaux Wetendorf[d], Chandra Yallampalli[e], William E. Gibbons[e], John P. Lydon[d], and Francesco J. DeMayo[b,2]

[a]Department of Obstetrics and Gynecology, University of North Carolina, Chapel Hill, NC 27599; [b]Reproductive and Developmental Biology Laboratory, National Institute of Environmental Health Sciences, Research Triangle Park, NC 27709; [c]Integrative Bioinformatic Support Group, National Institute of Environmental Health Sciences, Research Triangle Park, NC 27709; [d]Department of Molecular and Cellular Biology, Baylor College of Medicine, Houston, TX 77030; and [e]Department of Obstetrics and Gynecology, Baylor College of Medicine, Houston, TX 77030

Edited by R. Michael Roberts, University of Missouri, Columbia, MO, and approved January 19, 2021 (received for review June 6, 2020)

Uterine contractile dysfunction leads to pregnancy complications such as preterm birth and labor dystocia. In humans, it is hypothesized that progesterone receptor isoform PGR-B promotes a relaxed state of the myometrium, and PGR-A facilitates uterine contraction. This hypothesis was tested in vivo using transgenic mouse models that overexpress PGR-A or PGR-B in smooth muscle cells. Elevated PGR-B abundance results in a marked increase in gestational length compared to control mice (21.1 versus 19.1 d respectively, $P < 0.05$). In both ex vivo and in vivo experiments, PGR-B overexpression leads to prolonged labor, a significant decrease in uterine contractility, and a high incidence of labor dystocia. Conversely, PGR-A overexpression leads to an increase in uterine contractility without a change in gestational length. Uterine RNA sequencing at midpregnancy identified 1,174 isoform-specific downstream targets and 424 genes that are commonly regulated by both PGR isoforms. Gene signature analyses further reveal PGR-B for muscle relaxation and PGR-A being proinflammatory. Elevated PGR-B abundance reduces *Oxtr* and *Trpc3* and increases *Plcl2* expression, which manifests a genetic profile of compromised oxytocin signaling. Functionally, both endogenous PLCL2 and its paralog PLCL1 can attenuate uterine muscle cell contraction in a CRISPRa-based assay system. These findings provide in vivo support that PGR isoform levels determine distinct transcriptomic landscapes and pathways in myometrial function and labor, which may help further the understanding of abnormal uterine function in the clinical setting.

myometrium | progesterone receptor isoform | contractility | labor | parturition

Parturition-related disorders impact both maternal and neonatal health. Labor abnormalities such as postterm gestation and prolonged labor increase maternal and neonatal morbidity and complications (1, 2), while preterm birth (occurring <37 wk of gestation) complicates an estimated 15 million deliveries annually and ∼12% of all births worldwide (3–5). The resultant morbidity and mortality produce significant social and economic burdens for the care and support of preterm deliveries in the US health care system alone (4, 6).

Progesterone is necessary to maintain uterine quiescence and is now standard care for prevention of preterm labor in women with a history of premature delivery (7–9) by decreasing uterine contractility (8, 10–13). In many mammalian species, parturition is signaled by a significant decline in serum progesterone levels, thereby releasing the suppressive effect of serum progesterone on myometrial contraction (14–18). Humans, however, maintain high levels of progesterone throughout pregnancy and parturition (19–22), and the mechanisms of progesterone signaling in the myometrium are still unclear (11, 23–25).

The "progesterone receptor isoform switch" concept was posited to explain the transition from a quiescent to a contractile myometrial phenotype in the presence of high levels of progesterone (10, 11, 26–30). Progesterone acts via the nuclear receptor isoforms, PGR-A and PGR-B, which are coexpressed at different levels throughout pregnancy (31–35). Progesterone can transactivate different transcriptional programs determined by the relative levels of PGR-A and PGR-B isoforms in the myometrium (36–41). PGR-A can act in the same direction with—or, conversely, impose a dominant-negative effect on—PGR-B modulation of gene expression (40). In the myometrium of pregnant women, PGR-B is the dominant isoform during times of uterine quiescence and promotes anti-inflammatory actions (42). Studies have demonstrated that the PGR-B isoform mediates progesterone's progestational effects (42–44), and it is posited that in humans, contractility and myometrial inflammation is initiated by an up-regulation of PGR-A isoform's levels or activities (45–47). This increase promotes gene expression pathways that favor an inflammatory milieu (37, 48–52), such as oxytocin receptor (53) cyclooxegenase 2 (COX-2) (54) and

Significance

Preterm birth affects 10 to 12% of all pregnancies and is the primary cause of neonatal morbidity and mortality worldwide, while prolonged labor increases the risks of infection, uterine rupture, and neonatal distress. Progesterone suppresses uterine contractions. As humans maintain high levels of progesterone throughout parturition, a "functional progesterone withdrawal" hypothesis suggests that switching between myometrial PGR-A and PGR-B isoform activities is crucial for transitioning into the parturition mode. Our mouse models provide evidence in support of this hypothesis. These findings also demonstrate a significant difference in downstream transcriptomic landscapes between the two PGR isoforms. Therefore, this work opens a venue to investigate the PGR isoform interacting signaling for parturition control, providing a possible pathway for developing clinical therapies.

Author contributions: M.C.P., S.-P.W., C.Y., W.E.G., J.P.L., and F.J.D. designed research; M.C.P., S.-P.W., R.L., J.L., O.M.E., and J.P.L. performed research; S.-P.W. and M.W. contributed new reagents/analytic tools; M.C.P., S.-P.W., T.W., L.Z., C.Y., and J.P.L. analyzed data; and M.C.P., S.-P.W., T.W., L.Z., J.P.L., and F.J.D. wrote the paper.

The authors declare no competing interest.

This article is a PNAS Direct Submission.

[1]M.C.P. and S.-P.W. contributed equally to this work.

[2]To whom correspondence may be addressed. Email: francesco.demayo@nih.gov.

This article contains supporting information online at https://www.pnas.org/lookup/suppl/doi:10.1073/pnas.2011643118/-/DCSupplemental.

Published March 11, 2021.

prostaglandins (55, 56). Conversely, myometrium in women whose pregnancy is prolonged past term does not demonstrate this increase in PGR-A expression levels (57).

Previous work has included murine PGR-A and PGR-B whole mouse knockout models (35, 36) and cell culture models (42, 58–60). However, no in vivo models had been developed to test this intriguing hypothesis concerning the role of progesterone signaling in parturition (28, 61, 62). We describe here mouse models in which PGR-B or PGR-A levels are altered specifically within the myometrium and molecularly investigate the PGR isoform-specific effects on uterine contractility and the differences between these two isoforms on genomic regulation in an in vivo context.

Results

Increased Myometrial PGR-B Abundance Delays Parturition. The myometrial PGR isoform overexpression mouse models were established by crossing the Myh11Cre transgene (63) with either LSLPGR-A (64) or LSLPGR-B (65) conditional alleles. The Myh11 transgene is active in the ACTA2 positive myometrial smooth muscle cells, as demonstrated by the expression of green fluorescent protein that is encoded in the bicistronic open reading frame (*SI Appendix*, Fig. S1 *A–E*). The cre recombinase, driven by a *Myh11* promoter sequence, is able to activate the expression of transgenic PGR-A and PGR-B protein, which are detected by the MYC-tag at the N terminus of the transgenic proteins (*SI Appendix*, Fig. S1 *F* and *H*). Such activation is restrictive to the

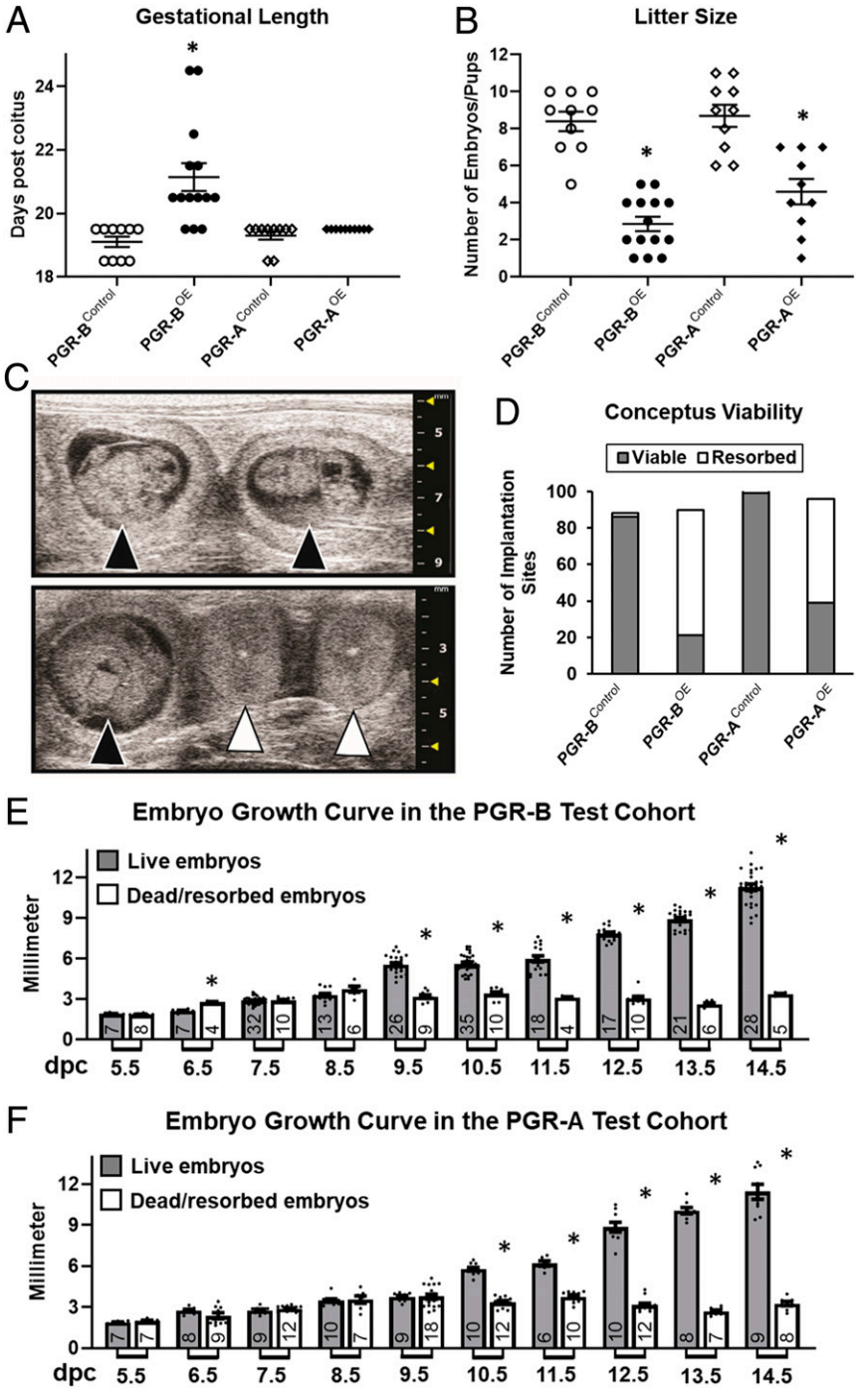

Fig. 1. Pregnancy impact by PGR isoform overexpression. (*A*) Gestational length and (*B*) litter sizes of the first litters from females of denoted genotypes. Gestation length is defined by the time of spontaneous parturition and ethics-related euthanasia. n = 10 (PGR-B^{Control}), 14 (PGR-B^{OE}), 10 (PGR-A^{Control}), and 10 (PGR-A^{OE}). *$P < 0.05$ in comparison with the corresponding control group by the two-tailed Mann–Whitney U test. (*C*) Representative ultrasound images of alive (black arrowheads) and resorbed (white arrowheads) embryos at 10.5 dpc. (*D*) Viability of embryos up to 18.5 determined by ultrasound. n = 88 (PGR-B^{Control}), 90 (PGR-B^{OE}), 103 (PGR-A^{Control}), and 96 (PGR-A^{OE}) total embryos examined. (*E* and *F*) Fetal growth curves in vivo by ultrasound. (*E*) Summary of PGR-B^{OE} and PGR-B^{Control} embryos. (*F*) Collective measurement of PGR-A^{OE} and PGR-A^{Control} fetuses. Filled bars denote viable fetuses and empty columns represent resorbed embryos. Numbers of datapoints are located at the bottom of each columns. Error bars denote SEM. *$P < 0.05$ between viable and resorbed embryos at the same gestation day by two-tailed Student's t test.

longitudinal and circular smooth muscle layers of the myometrium (*SI Appendix*, Fig. S1 *F* and *H*) but is absent in the endometrial epithelium and stroma (*SI Appendix*, Fig. S1 *G* and *I*). Activation of the PGR-A and PGR-B transgenes leads to expression of transgenic PGR-B (*SI Appendix*, Fig. S1*J*) and PGR-A (*SI Appendix*, Fig. S1*K*) proteins that have larger molecular weights than endogenous proteins because of the Myc-FLAG tandem tags (64, 65). Serum progesterone and estradiol levels at 13.5 d post coitum (dpc) are statistically comparable between overexpression and control mice (*SI Appendix*, Fig. S2 *A* and *B*). These results demonstrate that these two mouse models overexpress their respective PGR isoforms in the myometrial smooth muscle cells without perturbing serum pregnancy hormones.

Timed matings were employed to determine whether the PGR isoform overexpression dams show similar fecundity and gestational length compared to the control siblings. Prolonged gestational length was observed in 11 out of 14 examined PGR-B^{OE} mice (Fig. 1*A*). The gestation length was 19.10 ± 0.16 (PGR-B^{Control}), 21.14 ± 0.44 (PGR-B^{OE}), 19.30 ± 0.13 (PGR-A^{Control}), and 19.50 ± 0.00 (PGR-A^{OE}) d (Fig. 1*A*). Serum progesterone levels at term or postterm pregnancy were statistically comparable between PGR-B^{OE} and control groups (*SI Appendix*, Fig. S2 *C* and *D*). Marked maternal morbidity and mortality was observed in the PGR-B^{OE} dams with a 36% rate of maternal mortality on complications of labor dystocia requiring euthanasia of pregnant dams per ethical guidelines. The PGR-B^{OE} gestations were also associated with significant peripartum fetal mortality (5 out of 14 pregnancies). Conversely, PGR-A^{OE} females and their offspring did not have similar complications. PGR isoform overexpression also leads to fewer numbers of pups and late gestation fetuses with averages 8.41 ± 0.52 (PGR-B^{Control}), 2.86 ± 0.39 (PGR-B^{OE}), 8.70 ± 0.60 (PGR-A^{Control}), and 4.60 ± 0.69 (PGR-A^{OE}) at the end of pregnancy (Fig. 1*B*). High frequency ultrasound imaging revealed that the small litter size is because of early pregnancy failure in PGR-B^{OE} mice (69 of 90 embryos resorbed), compared to the 2 in 88 fetal resorption incidences in control mice (Fig. 1 *C* and *D*). Similarly, 57 of 96 embryos carried by PGR-A^{OE} mice were lost in comparison to 4 of 103 fetal loss in PGR-A^{Control} dams (Fig. 1*D*). The early pregnancy loss is further supported by the observation that a significant reduction of conceptus sizes occurred as early as 9.5 dpc and 10.5 dpc in the PGR-B and PGR-A test cohorts, respectively (Fig. 1 *E* and *F*). Total implantation sites exhibit no significant difference between control and overexpression groups in the PGR-A or PGR-B cohorts at first pregnancies, indicating that uterine receptivity was not affected by the myometrial overexpression of PGR isoforms (*SI Appendix*, Fig. S3). In summary, these findings demonstrate that only elevated PGR-B levels increased the incidence of prolonged gestational length, showing the differential impact on pregnancy between the two PGR isoforms. On the other hand, alterations in abundance of either one of these two PGR isoforms reduced embryo survivability in vivo, indicating a common effect of myometrial PGR-A and PGR-B dysregulation on fetal survival.

Elevated Myometrial PGR-B Levels Decreased in In Vivo Uterine Contractility. In agreement with the delayed parturition, labor dystocia, and morphological gross assessment, the in vivo uterine pressure measurements demonstrate decreased uterine tone and decreased uterine pressure during late gestation in the PGR-B^{OE} mouse (Fig. 2 and *SI Appendix*, Fig. S4). Using intrauterine telemeter pressure catheter recordings, the normal parturition of PGR-B^{Control} mice (n = 4) and abnormal parturition of PGR-B^{OE} mice (n = 5) was characterized before, during, and after parturition (or attempts at parturition in cases of labor dystocia) (*SI Appendix*, Fig. S4). The PGR-B^{OE} dams in this group had maternal death overnight 18.5 dpc (n = 2), labor dystocia postterm (n = 2), and delivery of a nonviable fetus (n = 1), which is reflective of the observed phenotype during the breeding trial.

Waveforms of pressure readings of PGR-B^{Control} parturitions were heterogeneous but overall reveal a pattern of marked increase in magnitude and frequency of contractions at the time of parturition (*SI Appendix*, Fig. S4*A*). This is in stark contrast to the waveforms of pressure readings of PGR-B^{OE} parturitions, which vary from minimal contractility to blunted contractile response pattern (*SI Appendix*, Fig. S4*B*). Overall, none of the PGR-B^{OE} parturitions are morphologically similar in appearance to the normal pattern of the PGR-B^{Control} parturitions (*SI Appendix*, Fig. S4 *A* and *B*). When the waveforms were carefully analyzed and enlarged as shown in a representative tracing (Fig. 2 *A* and *B*), the distinct increase in contractile amplitude in control parturition is readily apparent, with peak contractions more than 10-fold higher over baseline and a rhythmic pattern expected for expulsive efforts in labor (Fig. 2*A*). In contrast, the waveforms of pressure readings of PGR-B^{OE} parturition, as shown in a representative tracing in (Fig. 2*B*), the contractions are markedly blunted and weak, with only a twofold increase over baseline and less frequent. To quantify the contractile properties of PGR-B^{Control} and PGR-B^{OE} pregnancies, the pressures were analyzed for the 1 h of labor. PGR-B^{Control} dams are able to produce numerous contractions greater than 150 mmHg and 200 mmHg (Fig. 2*C*). In contrast, the PGR-B^{OE} pregnancies are significantly less capable to mount such high pressures (Fig. 2*C*). Moreover, the muscle of PGR-B^{OE} was significantly weaker after contractile exertion. The PGR-B^{OE} uterus could only maintain 70% of its initial strength after exposure to oxytocin, while the PGR-B control uterus was able to maintain complete uterine tone (Fig. 2*D*). These findings demonstrate a suppressive role of myometrial PGR-B on uterine contractility in vivo.

Differential Regulation of Uterine Tone and Stimulated Contractility by PGR-A and PGR-B. An assessment of uterine force, contractile strength, and frequency was determined via ex vivo assessment of isometric force. Isolation and stimulation of pseudopregnant mouse myometrium demonstrated that the PGR-B^{OE} uterine myometrial tone is lost at twice the rate compared to control uterus after being stretched with equivalent isometric force (Fig. 3*A*). Furthermore, when exposed to the uterotonic agent oxytocin at increasing concentrations, the PGR-B^{OE} uterus is not able to mount an appropriate contractile response compared to control myometrium (Fig. 3*B*). In contrast, PGR-A^{OE} uterine strips demonstrate a twofold increase in basal tone compared to PGR-A^{Control}, when equivalent isometric tension is applied to the myometrial specimens in the absence of uterotonic agents (Fig. 3*C*). Moreover, the PGR-A^{OE} myometrium demonstrates greater levels of sustained tone compared with the significant relaxation and fatigue observed in the control myometrium over the course of time (Fig. 3*C*). Additionally, PGR-A^{OE} myometrium demonstrate significantly increased contractility compared to control myometrium when stimulated by oxytocin (Fig. 3*D*). These results demonstrate that these two PGR isoforms modulate uterine contractility in an opposite manner.

Distinct Transcriptomic Profiles between PGR-A^{OE} and PGR-B^{OE} Uterine Tissues. RNA sequencing (RNA-Seq) assays were performed on uterine tissues of *Myh11Cre*, PGR-A^{OE}, and PGR-B^{OE} mice at 13.5 dpc to identify alterations of molecular pathways for the phenotypic changes. This stage was chosen based on results from reanalyzing previously published mouse myometrium transcriptomic data that show a majority of the significantly altered biological processes, reflected by changes on myometrial gene expression, between day 14 gestation and virgin myometrium (D14) can also be observed between day 18 gestation and virgin mice (D18) (Dataset S1) (66). Using an enrichment P value less than 0.05 to define significant overrepresentation, 94.9% of enriched gene ontology (GO) terms in D14 are also found in D18 (Dataset S1). Similarly, 91.9% of overrepresented biological processes in D14 are present in D18 based on the Molecular Signatures Database (MSigDB) (67) (Dataset S1). This finding not only

PHYSIOLOGY

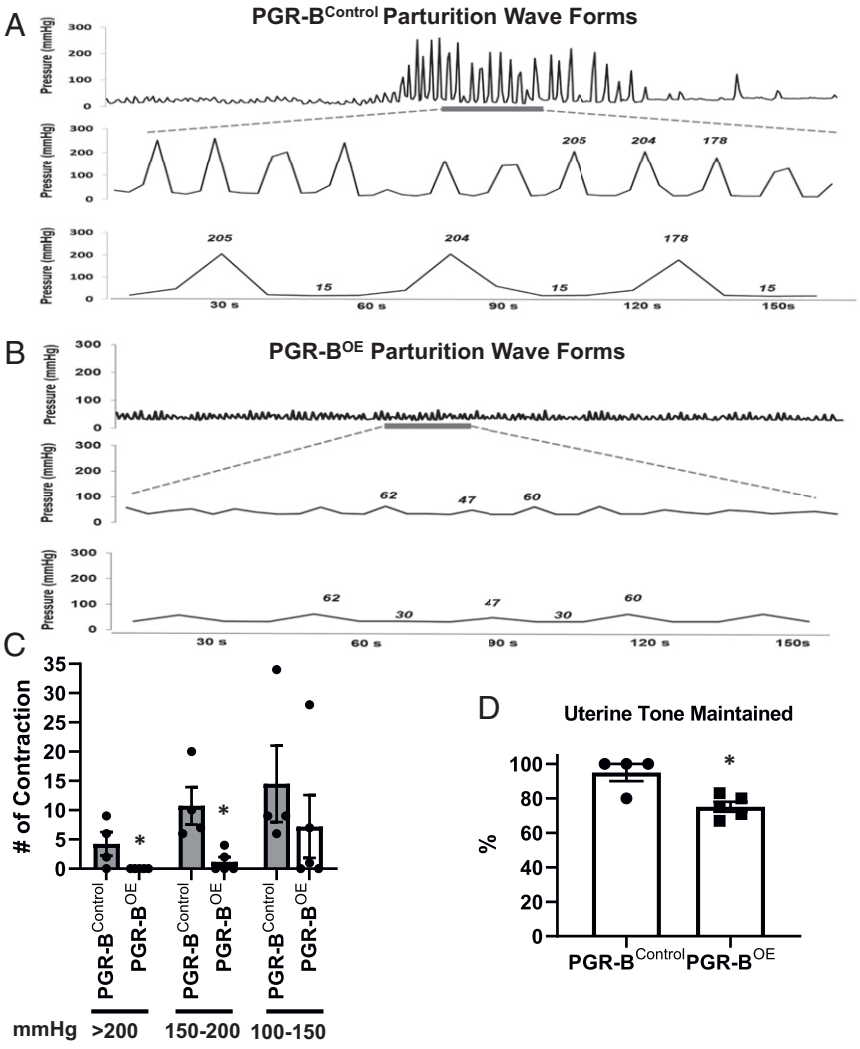

Fig. 2. Intrauterine pressure measurement. (*A* and *B*) Representative pressure wave recordings from PGR-B^{control} (*A*) and PGR-B^{OE} (*B*) dams. (*A*) A representative typical pressure waveform contraction pattern seen in control uteri. The intrauterine pressure measured in millimeters of mercury is seen increasing and decreasing as time continues on the *x*-axis, representing uterine contractions over time. The three waveform panels are the same control mouse parturition, with increasing magnification to appreciate the peaks and troughs of the laboring mouse pressure waveform contractions. (*B*) The pressure waveform pattern of PGR-B overexpressing uteri is shown for the same time intervals. The intrauterine pressure of the *y*-axis is measured in millimeters of mercury, with time during parturition on the *x*-axis. The three waveform panels of B are the same PGR-B overexpressing mouse parturition, with increasing magnification to appreciate the peaks and troughs of the laboring mouse pressure waveform contractions. (*C*) Numbers of distinct contractions in each category of intrauterine pressure levels, measured in millimeters of mercury (>200, 150 to 200, 100 to 150 mmHg, respectively). (*D*) Throughout the parturition attempt, the basal resting pressure of the uterus between contractions was compared to the original basal pressure; the percentage of uterine tone maintained at the end of parturition was determined for control and overexpressing; a lower percentage uterine tone maintained represented decreased basal uterine pressure over time. $n = 4$ (PGR-B^{control}) and 5 (PGR-B^{OE}). $^*P < 0.05$ in comparison with the corresponding control group by two-tailed Mann–Whitney *U* test. Error bars denote SEM.

indicates that most molecular changes toward term pregnancy already manifest or are in the process to commence at midpregnancy but also suggests that examining uterine transcriptome profiles at 13.5 dpc would allow molecular assessments on genomic alterations that lead to subsequent physiological changes.

Overall expression of *Pgr-A* and *Pgr-B*, as determined by the common sequence of *Pgr* isoforms in exon 2, increased from 5.83 ± 1.18 normalized read counts in the control to 32.73 ± 4.01 for PGR-A^{OE} and 33.75 ± 4.43 for PGR-B^{OE} (*SI Appendix*, Fig. S5*A*), reflecting a significant increase of *Pgr* transcripts in both overexpression groups. The performance of these two transgenes appeared comparable with no statistical difference between their normalized read counts (*SI Appendix*, Fig. S5*B*), which is consistent with our previous observations on in the PgrCre-activated models (68). These results demonstrate that both transgenes can achieve an average fivefold of overexpression in comparison to the endogenous *Pgr* locus.

Using FPKM (fragments per kilobase of exon per million reads mapped) greater or equal than one in any of the four samples in each group as the cutoff, we found expression of 12873, 13117, and 12990 genes in the *Myh11Cre*, PGR-A^{OE}, and PGR-B^{OE} tissues, respectively (Dataset S2). Among these three groups, 12569 genes are commonly expressed (Dataset S2). These observations suggest that the impact of PGR-A and PGR-B overexpression is mostly at regulating the level of expressing genes. Compared with the *Myh11Cre* control, the PGR-A overexpression resulted in alterations of 941 genes, 562 up and 379 down, with the cutoff of absolute fold changes greater or equal to 1.3 and unadjusted $P < 0.05$ (Fig. 4*A* and Dataset S3). Using the same criteria, we found that increased PGR-B expression leads to 564 gene changes with 348 up and 216 down at midpregnancy (Fig. 4*A* and Dataset S3). Between the PGR-A^{OE}– and PGR-B^{OE}–dependent differentially expressed genes (DEGs; PGR-A^{OE_DEG} and PGR-B^{OE_DEG}, respectively), 230 of the total 231 genes are regulated by the two PGR isoforms in the same direction, while only the *Aldh1a7* gene is suppressed by PGR-A and promoted by PGR-B (Fig. 4*B* and Dataset S3). In addition, 710 of the 941 PGR-A^{OE_DEG} and 333 of the 564 PGR-B^{OE_DEG} are uniquely regulated by the respective PGR isoforms (Fig. 4*A* and Dataset S3). These findings demonstrate that the majority (82%) of downstream targets of PGR-A and PGR-B isoforms manifests isoform-specific regulation of expression.

The global impact of PGR isoforms on pregnancy-prompted myometrial remodeling were further evaluated by comparing enriched molecular pathways and biological processes of D14 (Dataset S1) with those of PGR-A^{OE} and PGR-B^{OE} (Dataset S4). Results from GO terms, MSigDB, and Ingenuity Pathway Analysis (IPA) diseases and functions databases show that PGR-A and PGR-B together control 57.24, 34.59, and 68.4%, respectively, of annotated pathways/processes that are altered in the myometrium between day 14 gestation and virgin (Fig. 4 *C*–*E*). While up to 39.4% of myometrial remodeling pathways

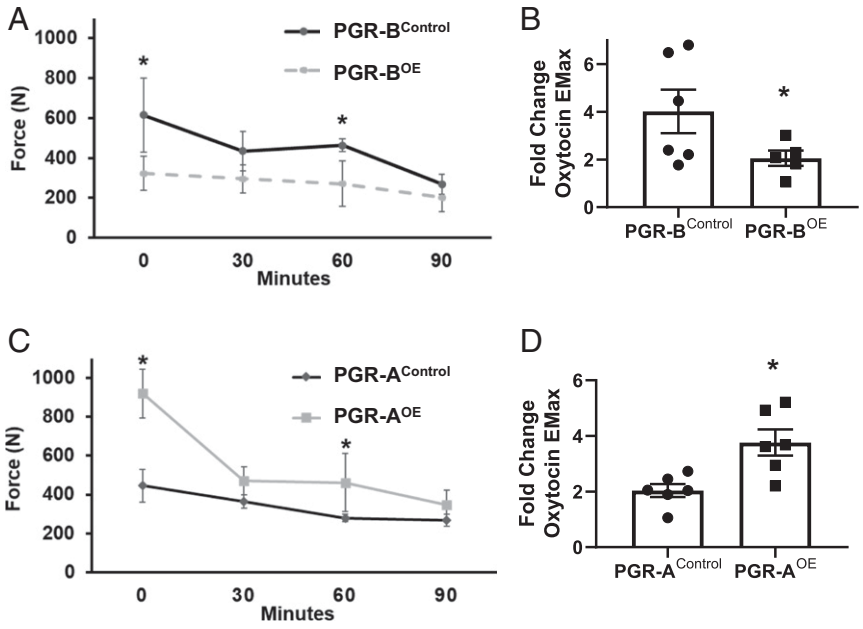

Fig. 3. Ex vivo contractility of isolated uterine strips. (*A* and *B*) PGR-B cohorts. (*C* and *D*) PGR-A tissues. The baseline resting uterine tone over time (minutes) was determined in 30 min intervals in PGR-B^{OE} (*A*) or PGR-A^{OE} (*C*) tissues. The contractile responses of uterine tissue to oxytocin at maximum effect (EMax 10^{-7} M) were compared to baseline unstimulated uterine tone in PGR-B^{OE} (*B*) or PGR-A^{OE} (*D*) tissues. *$P < 0.05$ by one-way ANOVA test for repeated measures. Error bars denote SEM.

and processes are linked to both PGR-A and PGR-B, an average of 17.68 and 9.48% are specifically associated with PGR-A and PGR-B, respectively (Fig. 4 *C–E*). These data reveal the extensive control of PGR-A and PGR-B isoforms on the molecular programs in the myometrium that are adaptive to pregnancy.

Distinct functions of the PGR-A and PGR-B isoforms were further assessed by examining the enrichment of functional and disease annotations of the 941 PGR-A^{OE_DEG} and 564 PGR-B^{OE_DEG}. Presumptive activities of molecules that are upstream of PGR-A and PGR-B target genes were also estimated via the IPA Upstream Regulator analysis. Multiple categories of biological processes including "recruitment of leukocytes," "glucose metabolism disorder," "neovascularization," and "growth of connective tissue" show opposite directionalities between PGR-A^{OE_DEG} and PGR-B^{OE_DEG}, based on the z-scores (Table 1 and Dataset S4). PGR-A controlled genetic programs that are positively associated with leukocyte recruitment and glucose metabolism, while PGR-B's gene signature was associated with blood vessel formation and connective tissue growth (Table 1). Using the PGR-A^{OE_DEG} and PGR-B^{OE_DEG} as reporters to estimate changes of molecular activities, IPA predicted that the PGR-A^{OE_DEG} gene signature resembles activation of interleukin 1 beta, tumor necrosis factor, and NF*k*B complex as well as an increase in use of glucose (Table 1). Conversely, the PGR-B^{OE_DEG} profile featured rose glucocorticoid signaling, simulated responses of losartan potassium and Rho kinase inhibitor Y-27632 treatment, and an increase of lipase E activities (Table 1). These results collectively indicate that PGR-A is proinflammation while PGR-B supports muscle relaxation. Also, these data further suggest divergent preferences of fuel usage between PGR-A and PGR-B isoforms in the myometrium.

PGR-B–Specific Regulation of the *Oxtr-Plcl2-Trpc3* Pathway for Smooth Muscle Contraction. The RNA-Seq data reveals PGR-B–dependent regulation of oxytocin receptor (*Oxtr*), phospholipase C-like 2 (*Plcl2*), and transient receptor potential cation channel subfamily c member 3 (*Trpc3*) that are in the same pathway for muscle contraction control (Dataset S3 and *SI Appendix*, Fig. S6*A*). The qRT-PCR assay validated the repression of *Oxtr* and *Trpc3* gene expression by PGR-B but not by PGR-A (*SI Appendix*, Fig. S6 *B* and *C*). On the other hand, the *Plcl2* gene that encodes the predominant paralog of phospholipase C-like proteins in mouse uteri exhibited higher messenger RNA (mRNA) and protein levels only in the PGR-B^{OE} group (Fig. 5 *A* and *B* and Dataset S2). Furthermore, the similar gene signatures between PGR-B^{OE_DEG} and losartan potassium treatment suggest a change of activities in the phospholipase C signaling pathway that is employed by both oxytocin and angiotensin signaling (*SI Appendix*, Fig. S6*A*) (69, 70). These results collectively demonstrate that PGR-B modulates gene expression of effectors and activities of the *Oxtr-Plcl2-Trpc3* pathway.

Since both *Oxtr* and *Trpc3* are already known to positively regulate myometrial contraction (69, 71), PLCL2 and its paralog PLCL1 were subject to the collagen gel contraction assay to examine their functionality on myometrial cell contraction (72). Overexpression of PLCL1 (PLCL1^{OE}) and PLCL2 (PLCL2^{OE}) in uterine smooth muscle hTERT-HM cells was mediated by locus-specific guide RNAs in a CRISPR activation (CRISPRa) system (58, 73). Compared with the scrambled guide RNA transduced cells (control), *PLCL1* and *PLCL2* guide RNAs effectively and selectively increased both mRNA and protein expression of endogenous *PLCL1* and *PLCL2* genes, respectively, (*SI Appendix*, Fig. S7 *A–C*). Abundance of smooth muscle marker genes ACTA2 and TAGLN are comparable among PLCL1^{OE}, PLCL2^{OE}, and control cells (*SI Appendix*, Fig. S7 *D* and *E*), suggesting that both PLCL1 and PLCL2 overexpression cells maintained the smooth muscle phenotype. In collagen gels, both PLCL1^{OE} and PLCL2^{OE} manifested significantly larger diameters than the control group under oxytocin stimulation (Fig. 5 *C* and *D*). These findings reveal the role of phospholipase C-like proteins in suppressing uterine smooth muscle contraction with a human relevance. In summary, our data show the PGR-B–specific modulation on multiple regulators in a signaling cascade for muscle contraction that includes the oxytocin receptor, the phospholipase C signaling, and a calcium channel of known contribution on laboring (69, 71, 74).

Manifestation of PGR Isoform Gene Signatures in Human Myometrial Specimens. The mouse uterine PGR-A^{OE_DEG} and PGR-B^{OE_DEG} gene signatures enabled the evaluation of these two PGR isoforms' activities in human myometrial tissues. PGR isoform gene signatures were used to assign each patient's transcriptomic profile a t-score as a surrogate of the PGR isoform activity (75). The estimated PGR-A activity, as reflected by the t-scores, is

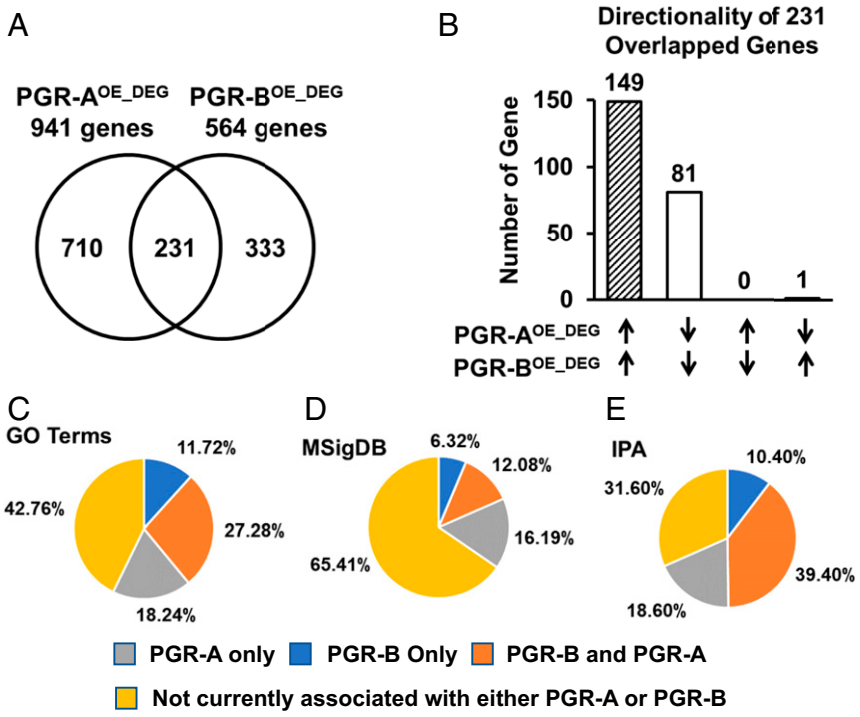

Fig. 4. Transcriptomic profiles of PGR-A and PGR-B overexpression uteri. (*A*) Common and distinct genes that are modulated by PGR-AOE and PGR-BOE in comparison to the Myh11Cre, respectively, shown in a Venn diagram. (*B*) A comparison on the effect of PGR-A– and PGR-B–dependent gene regulation in the 231 genes whose expression were altered by both PGR isoforms. (*C–E*) Percentages of enriched myometrial remodeling biological processes in association with PGR-A– and PGR-B–dependent genome regulation. Overrepresentation of gene annotations was determined by GO (*C*), MSigDB canonical pathways (*D*), and IPA Diseases and Functions (*E*). Differentially expressed genes between gestation day 14 and virgin mouse myometrium (GSE17021) were used to identify enriched myometrial remodeling biological processes.

statistically higher in term pregnant specimens compared with nonpregnant human myometrial specimens (Fig. 6*A*) (76), while t-scores of the PGR-B gene signature did not show a significant change between these two groups (Fig. 6*B*). The increased myometrial PGR-A activities at term suggests that the human myometrium adopts a transcriptomic profile at term in favor of muscle contraction to prepare for parturition.

Next, we estimate the fraction of myometrial remodeling-related molecular events that are associated with PGR-A and PGR-B isoforms. Enriched pathways/processes, based on altered expression of genes between term pregnant and nonpregnant human myometrial tissues, were identified by the three aforementioned databases (Dataset S5) (76), which were followed by comparing with mouse-based PGR isoform-dependent proceedings (Dataset S4). Among which, up to 39.2% of pathways and processes are known to be regulated by PGR-A and PGR-B, while those linked only to PGR-A or PGR-B constitute an average of 18.4 and 9.48% of annotated molecular events (Fig. 6 *C–E*). The similar pattern between human and mouse (Fig. 4) observations suggests that PGR-A and PGR-B may also impose regulations on common and distinct molecular processes in the human myometrium in a wide spectrum.

Discussion

Modeling Progesterone Isoforms Functions In Vivo. Although the consequences of preterm births have significant economical and societal burdens, the molecular mechanisms controlling the timing of parturition are poorly understood. Human studies establish correlative indications between genes and physiological presentations (12, 33, 37, 77), while in vitro human myometrial cell culture models further shed light on candidate molecular pathways (42, 60). Moreover, physiological tests by previous mouse models have not used uterine tissue-specific tools to selectively

Table 1. Molecular functions of PGR isoform targets by IPA

	PGR-A^{OE_DEG}		PGR-B^{OE_DEG}	
	Activation *z*-score	*P* value of overlap	Activation *z*-score	*P* value of overlap
Function/disease				
Recruitment of leukocytes	2.0	1.18×10^{-7}	−0.35	5.00×10^{-9}
Glucose metabolism disorder	1.60	2.02×10^{-18}	−0.94	6.63×10^{-13}
Neovascularization	−0.12	2.73×10^{-6}	1.83	5.78×10^{-7}
Growth of connective tissue	−0.92	2.66×10^{-6}	1.55	7.10×10^{-8}
Molecular activities				
IL1β	1.99	2.27×10^{-13}	0.54	2.45×10^{-12}
TNF	2.34	6.54×10^{-14}	0.29	5.57×10^{-10}
NFkB (complex)	2.32	1.26×10^{-7}	0.54	1.21×10^{-7}
Glucocorticoid	−1.01	4.23×10^{-4}	1.38	8.56×10^{-4}
Losartan potassium	—	—	0.99	1.60×10^{-5}
Y-27632	−1	1.11×10^{-2}	0.80	9.80×10^{-3}
D-glucose	2.21	1.40×10^{-9}	0.06	4.37×10^{-6}
LIPE	—	3.90×10^{-5}	2.41	2.95×10^{-7}

IL1β: interleukin 1 beta; TNF: tumor necrosis factor; NFkB: nuclear factor kappa-light-chain-enhancer of activated B cells; LIPE: lipase E.

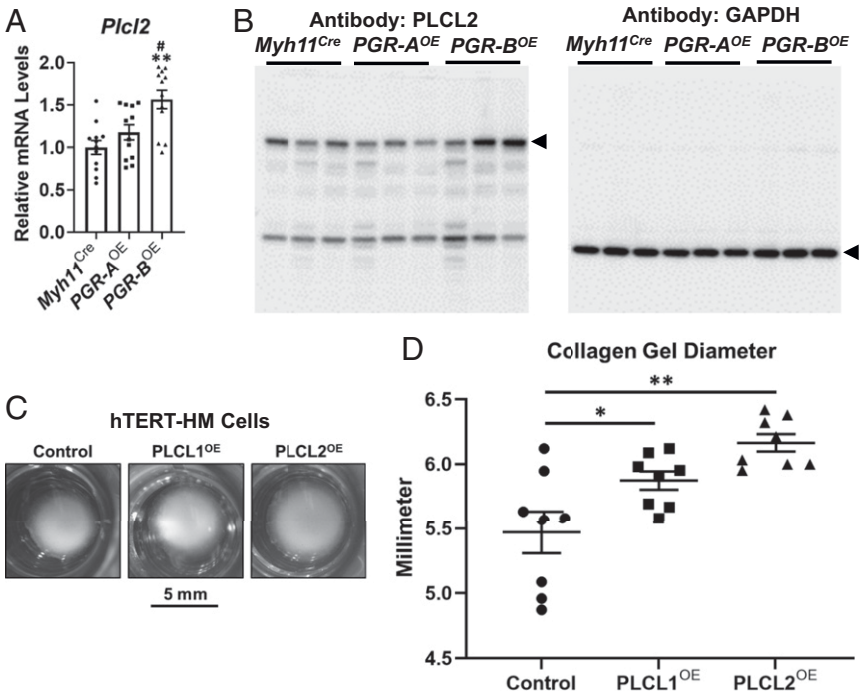

Fig. 5. Regulation and functionality of phospholipase C-like genes. (*A* and *B*) mRNA abundance (*A*) and protein levels (*B*) of *Plcl2* in denoted genotypes. $^{**}P < 0.01$ compared with the *Myh11*^{Cre} group. #, $P < 0.05$ compared with the *PGR-A*^{OE} group. For mRNA, each group had six biological replicates, and each biological replicate had two PCR technical duplicates. Error bars denote SEM. For the Western blots, GAPDH serves as the loading control of Western blot assay. Arrowheads mark the bands of annotated protein sizes in mice. (*C* and *D*) Representative images (*C*) and diameters of collagen gels (*D*) from the cell contraction assay on hTERT-HM cells of denoted manipulations of gene expression. $^{*}P < 0.05$ and $^{**}P < 0.01$. Two-tailed Mann–Whitney *U* test was used.

separate PGR-B and PGR-A expression to the myometrial compartment (35, 36, 78). With spatiotemporal specificity defined by the endogenous smooth muscle promoter (63, 79), we have effectively targeted the overexpression of PGR-B and PGR-A to only the smooth muscle compartment, allowing us to address a long-standing hypothesis in parturition biology that changes in the expression levels of myometrial PGR-B, and PGR-A controls timely delivery (37, 45–47).

Our previous findings and data in this study show successful activation of LSLPGB-A and LSLPGR-B minigenes by PGRCre (64, 68), Wnt7aCre (64), MMTVCre (65), and Myh11Cre (*SI Appendix*, Fig. S1) in various cell types, which demonstrate the reliability of this Cre-activated overexpression system. Moreover, overexpression of one PGR isoform does not increase the level of the other one (*SI Appendix*, Fig. S1 *J* and *K*) (65, 68). This feature enables the capture of specific isoform activities with reduced noise from the other isoform. Notably, variations on the transgene expression do exist, ranging between 20.8 and 29.8 normalized read counts for PGR-B^{OE} and from 16.3 to 29.3 in the PGR-A^{OE} group (*SI Appendix*, Fig. S5*B*). These variations could potentially contribute, in part, to the spectrum of increased gestation length in the PGR-B^{OE} mice (Fig. 1*A*). Whether there is a linear correlation between gestation length and PGR-B levels would be better investigated in the future with mice in a pure genetic background.

The significant loss of embryos in PGR-A^{OE} and PGR-B^{OE} groups could result from the defective egg/embryo transportation mechanism between ovaries and the uterus. Rhythmic oviduct contractions, pivotal to moving embryos, depend on the homeostasis of oviduct muscularis (80). The observations that PGR isoform overexpression altered smooth muscle contractility (Fig. 3) implicate potential disruption of coordinated oviduct contraction by aberrant changes of PGR isoform activities. Such disruption could potentially affect the timing of embryos' arrival in the uterus at the window of receptivity. Embryos missing the window of receptivity may still proceed to implantation but often end up with pregnancy loss (81). Another potential cause of the pregnancy loss phenotype is the spiral vasculature remodeling (82). In our model, the *Myh11Cre* allele does not appear to activate the transgene in vascular smooth muscle cells (VSMCs) inside the myometrial compartment, evident by the lack of PGR immunoreactivity in myometrial VSMCs (*SI Appendix*, Fig. S1*H*). This could result from the very low Myh11Cre expression in VSMCs of the uterine compartment as seen in the lack of colocalization of smooth muscle alpha actin and Myh11Cre allele driven enhanced green fluorescent protein (eGFP) (*SI Appendix*, Fig. S1*E*). Based on this observation, PGR isoform overexpression is less likely to impact spiral artery remodeling in a cell autonomous manner. Whether the myometrial PGR overexpression may act in other capacities to affect the spiral vasculature remains to be investigated (82).

While *Myh11* gene expression is detected in mouse ovaries (83), the comparable total implantation sites among control and overexpressors suggest that both PGR-A and PGR-B overexpressors' ovaries were competent in ovulation (*SI Appendix*, Fig. S3). In addition, the serum progesterone and estrogen levels show no statistical differences between control and overexpressors at 13.5 dpc (*SI Appendix*, Fig. S2). Furthermore, PGR-B overexpressors did not show clustered deviations of serum progesterone levels at term and postterm from control mice (*SI Appendix*, Fig. S2 *C* and *D*). These results collectively suggest that the ovarian functions of the PGR-B overexpressor remain capable for pregnancy.

Ligand interaction has been shown to impact PGR isoform actions in human myometrial cells and is associated with preterm labor (30). In our models, serum progesterone levels manifested no statistical difference between PGR-B^{OE} and control groups at term or postterm pregnancy (*SI Appendix*, Fig. S2 *C* and *D*). This data suggests that the progesterone supply from the blood was not affected in the overexpression models. Future experimentations are warranted to examine the local progesterone and the key progesterone metabolizing enzyme 20α-hydroxysteroid dehydrogenase (*Akr1c18*) levels for further exploring the ligand interaction mechanism, even though *Akr1c18* mRNA levels were not altered by PGR isoform expression in 13.5 dpc uterine tissues (Dataset S3).

PGR-B and PGR-A Have Opposing Actions on Myometrial Contractility. Our first line of investigations reveals that elevation of myometrial PGR-B or PGR-A levels result in marked abnormalities

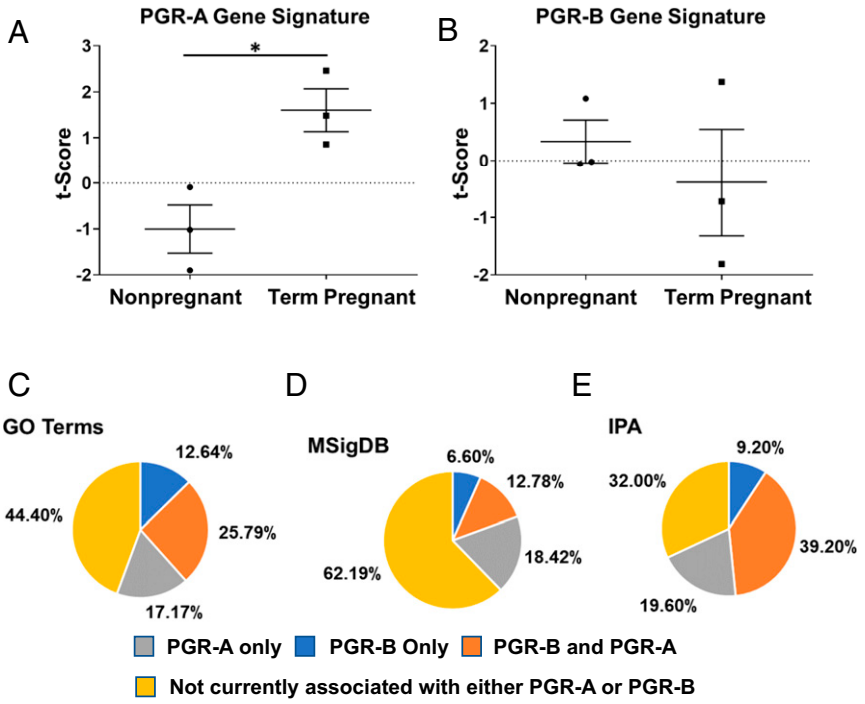

Fig. 6. PGR-A^{OE_DEG} and PGR-B^{OE_DEG} gene signatures in human myometrial tissues. (*A* and *B*) t-scores of the denoted gene signatures, as surrogates of PGR-A (*A*) and PGR-B (*B*) molecular activities, in nonpregnant and term pregnant myometrial specimens (GSE137551). *$P < 0.05$ by two-tailed unpaired *t* test with Welch's correction. Error bars denote SEM. (*C*–*E*) Percentages of enriched myometrial remodeling-related molecular processes in association with PGR-A– and PGR-B–dependent genome regulation. Differentially expressed genes between term pregnant and nonpregnant human myometrium (GSE137551) were used to identify enriched myometrial remodeling biological processes.

in parturition and myometrial contractility. As expected, overexpression of PGR-B in the mouse myometrium results in a significant increase in gestational length and the inability for the uterus to successfully expulse the pregnancy in a timely manner. Furthermore, sophisticated in vivo analysis clearly demonstrates that PGR-B overexpression is associated with decreased intrauterine pressure and an abnormal labor pattern. This is significant, as it is a demonstration of a marked biological effect of PGR isoforms on parturition. These in vivo findings are further reinforced by well-controlled ex vivo dose–response curves, which demonstrate a significantly low contractile response when PGR-B is overexpressed. Importantly, while overexpression of PGR-B results in the predicted "relaxed" myometrial phenotype that is unable to contract in response to oxytocin, the overexpression of myometrial PGR-A demonstrated the predicted "contractile" myometrial phenotype with a twofold increased contractility in response to uterotonic agents.

In addition to the uterine myometrium, PGR isoforms could also work in a similar manner on oviduct smooth muscle. Coordinated muscle contraction and relaxation in the oviduct deliver embryos to the uterus in time at the window of receptivity, and disruption of this orchestrated muscle movement results in early pregnancy loss (80). Manifestation of the growth arrest phenotype in PGR-A^{OE} and PGR-B^{OE} pregnancy (Fig. 1) implicates a role of PGR in the oviduct, which warrants future investigations.

PGR-B and PGR-A Differentially Regulate Key Molecular Pathways. Transcriptomic data further support the differential regulation of crucial factors which control uterine contractility and parturition, as multiple well-characterized signaling pathways are differentially manifested in uteri overexpressing the PGR-A or PGR-B isoform. Oxytocin signaling through its receptor (OXTR) is a recognized, critical element to promote myometrial contractility in human labor (84). Our molecular evidence demonstrates that *Oxtr* is significantly lower in PGR-B overexpressing mice, providing a functional basis by which these mice are unable to mount a contractile response to oxytocin in well-controlled ex vivo experiments. Lipopolysaccharide (LPS) is well established in the promotion of an inflammatory pathway associated with parturition and is widely used to induce labor in mice (60, 85). Our findings reveal that PGR-A–dependent transcriptome is more associated with LPS treatment than PGR-B (Dataset S4), suggesting an elevated inflammation baseline set by the increased PGR-A/PGR-B ratio. This observation also provides compelling evidence that PGR isoforms differentially influence crucial inflammatory pathways that are well established in human and murine parturition.

Interestingly, the gene expression profiles of myometrial PGR-A and PGR-B overexpression exhibit differences in estimated mitogen-activated protein kinase (MAPK) activities (Dataset S4). Pharmacological inhibition of MAPK activation in mice is known to suppress oxytocin-induced cyclooxygenase-2 and prostacyclin levels in human myometrial cells (86). The differential MAPK activities under the varying PGR isoform ratios may allow modulation of progestational signaling that controls the state of uterine relaxation in these mice.

The transforming growth factor-beta (TGFβ) superfamily of proteins is well characterized in pregnant human myometrium and is thought to play a role in preparing the myometrium for parturition (87–89). Interactions between progesterone and TGFβ signaling on gene regulation have been reported in uterine and lung cells (90, 91). Our data suggest that TGFB1 activities may be under the influence of myometrial PGR isoforms, with higher estimated TGFB1 activities in PGR-A overexpressing uteri than PGR-B (Dataset S4). This predicted difference in TGFB1 activities may represent a novel regulatory pathway under control of PGR isoforms in the uterus. Future investigations into the specific molecular mechanisms of PGR control over oxytocin, TGFβ, and LPS-induced contractility will help clarify the specific molecular interactions among these pathways.

The differences on predicted activities of glucose and lipase E implicate the versatile function of PGR in regulation of energy metabolism through utilizing different PGR isoforms (Table 1). In human myometrium, transcriptomic profiles project an increase of glucose utilization at term pregnancy compared to the nonpregnant state (76), concomitant with the increased PGR-A over PGR-B ratio toward term (37). This estimated higher usage

of glucose by PGR-A overexpressing mouse uteri is similar to observations in the human myometrium, highlighting the functional correlation between species in late gestation.

Regulation of Catalytic Inactive Phospholipase C-Like Proteins by PGR. The phospholipase C pathway mediates extracellular signals to release intracellularly stored calcium leading to muscle contraction. The PGR-B isoform-dependent transcription program sets a framework that restricts signaling capacity of the phospholipase C pathway to mediate contractile stimulation (Fig. 5). Among the member genes in this pathway, *Plcl2* encodes a catalytically inactive form of the phospholipase C family of proteins that bind to phospholipid phosphatidylinositol 4,5-bisphosphate (PIP2) and the second messenger inositol 1,4,5-trisphosphate (IP3) (92, 93). The phospholipase C-like proteins PLCL1 and PLCL2 are thought to act as sequesters of inositol triphosphates and reduce the signal to release calcium from the intracellular calcium storage (93), thereby negatively regulating calcium signaling (94, 95). Known functional indications of PLCL proteins include energy metabolism, neuron transmission, cancer metastasis, immune response, and bone formation (95–98). For female reproduction, loss of both *Plcl1* and *Plcl2* results in subfertility, abnormal estrous cycle, and smaller uteri in mice (99). *PLCL1* expression is dominant in human myometrium (76), while *Plcl2* mRNA levels are much higher than *Plcl1* in the mouse uteri (Dataset S2). We and others show that human myometrial PLCL1 attenuates muscle cell calcium movement and contractility (Fig. 5*D*) (100). Progesterone increases *PLCL1* expression in the human endometrial stroma cell model (94), and PGR occupancy has been identified near the PLCL1 genomic locus in human myometrial tissues (76). These findings suggest a negative regulatory role for progesterone signaling in the phospholipase C pathway in human uterine tissues, which aligns with the silencing effect of progesterone on myometrial contractility. The present study further demonstrates that PGR-B isoform exerts such repressive function through the dominant PLCL isoform *Plcl2* in the mouse myometrium (Fig. 5 *A* and *B*). Similar to PLCL1, PLCL2 also blunts myometrial cell contraction (Fig. 5*D*). PGR occupies the PLCL2 promoter and upstream intergenic regions (76), suggesting a potential direction transcription regulation of PLCL2 by PGR. The mechanism by which PLCL2 modulates smooth muscle cell contractility remains unclear and awaits future experimentations.

Materials and Methods

Animals. Myh11Cre mice [B6.Cg-Tg(Myh11-cre,-EGFP)2Mik/J] were acquired from the Jackson Laboratory (stock no.: 007742) (63). LSLPGR-A and LSLPGR-B mice were generated in-house and are described elsewhere (64, 65). Mice were maintained in a recurrent photocycle of 12 h on–off in temperature-controlled rooms within an American Association for Accreditation of Laboratory Animal Care accredited vivarium at the Baylor College of Medicine and the National Institute of Environmental Health Sciences. Animal handling and procedures were performed following the guidelines detailed in the *Guide for the Care and Use of Laboratory Animals* (101). All procedures were approved by the Institutional Animal Care and Use Committee at Baylor College of Medicine under animal protocol number AN-4203 and by the Institutional Animal Care and Use Committee at the National Institute of Environmental Health and Sciences under protocol number 2015–0012.

Breeding pairs were placed together at 1700 hours and separated by 0700 hours the following morning, which was designated 0.5 dpc; gestational length was subsequently recorded as dpc. Parturition was recorded upon delivery of the first pup or presence of a litter at 0700 hours; pups were counted, assessed for viability, and weighed following birth.

Ultrasound Imaging. High frequency ultrasound was used to measure fetal viability and growth throughout gestation as previously described (102). Dams were anesthetized during gestation beginning at 5.5 dpc (2% isoflurane; 100% oxygen). Abdominal hair was removed with depilatory cream. Dams were positioned supine to monitor heart rate and body temperature. Implantation site locations, embryo viability, and fetal size were visualized using the VisualSonics Vevo 2100 Imaging System with 550s scan head (FUJIFILM VisualSonics Inc.) (102). Fetal viability was documented by cardiac activity via M-mode Doppler at 9.5 dpc. Intrauterine fetal death was diagnosed as no fetal heartbeat observed for greater than 60 s on ultrasound imaging. After completion of imaging, dams were monitored until fully recovered from anesthesia. The development and monitoring of fetal growth from 5.5 dpc through 9.5 dpc can be detected, while documentation of cardiac activity at 9.5 dpc is possible.

Gross Tissue Specimen Analysis. Mice were euthanized by cervical dislocation after anesthesia was obtained in automated CO_2 euthanasia chambers (Euthanex). Through an abdominal incision, the reproductive tract including the upper vagina, cervix, bilateral uterine horns, and bilateral ovaries was then surgically excised, examined, and photographed. Gross tissue specimen analysis was used to assess uterine morphology during pregnancy and to corroborate ultrasound findings. The compilation of these data allows development of a type of "virtual mapping" and reconstruction of the pregnant mouse uterus in silico.

Uterine Isometric Contractility Analysis. At 6.5 dpc of pseudopregnancy, mice were euthanized, and the entire uterus was excised. The uterine horns were immediately immersed in oxygenated Krebs physiological saline solution (119 mM NaCl, 4.7 mM KCl, 2.5 mM $CaCl_2$, 1.17 mM $MgSO_4$, 25 mM $NaHCO_3$, 1.18 mM KH_2PO_4, 0.026 mM ethylenediaminetetraacetic acid, and 5.5 mM D-glucose). Next, uterine strips (5 × 2 mm) were mounted on a wire myograph (Danish Myograph Technology), placed under 1 g of tension in a bath of Krebs solution, and equilibrated for 30 min using LabChart software (ADInstruments).

After a baseline integral value of unstimulated uterine tone was recorded, the uterine strips were exposed to increasing concentrations of oxytocin (10 to 8.5 M to 10 to 6 M, Sigma-Aldrich), and concentration–response curves were recorded to determine maximum effect dose. Responses are presented as the integral value over a period of 10 min and normalized to each individual strip's baseline integral value at 1 g tension. The baseline resting uterine tone over the duration of exposure to oxytocin was also recorded.

Statistical analysis for the ex vivo contractility assays utilized the One-Way ANOVA Calculator for Repeated Measures from Social Science Statistics (https://www.socscistatistics.com/).

In Vivo Telemetry Surgical Implantation Procedure. Mice were mated at 6 to 8 wk of age, and PGR-B^{LSL} littermates of PGR-B^{OE} mice served as controls. The PhysioTel PA-C10 Transmitter (Data Sciences International [DSI]) was used to measure intrauterine pressure before, during, and after parturition, as previously described and demonstrated (103, 104). Prior to surgery, the dams were confirmed pregnant, and the number of pups in each uterine horn was counted via high frequency ultrasonography (102). At 10.5 dpc, dams were weighed and injected subcutaneously with slow-release buprenorphine (0.6 mg/kg) 30 min prior to surgery. Animals were anesthetized with 2% isoflurane in 100% oxygen.

With an aseptic and sterile technique, a 1 cm vertical incision was made in the abdominal wall. The right uterine horn was identified, and a small 1 mm incision was made at the most distal portion of the uterine horn. Small surgical forceps were used to insert the pressure catheter between the uterine wall and fetus, attempting to not rupture the amniotic membrane. The catheter was visualized to pass through the most distal pregnancy and then progressed further proximally toward the cervix with light pressure so as to enter at least the second pregnancy site. Next, a small drop of Vetbond surgical glue (3M) was applied to the site of uterine insertion and allowed to dry. The PA-C10 Transmitter and implanted horn were returned to the body cavity. The peritoneum was sutured in a running fashion with 5-0 Vicryl, and the abdominal wall was sutured with 6-0 Monocryl in an interrupted fashion; the mouse was monitored until awake.

In Vivo Telemetry Parturition Data Acquisition and Analysis. Telemetry recordings were performed with the Dataquest ART data acquisition system, version 4.10 (DSI); each mouse was maintained in the cage and placed on the recording receiving pad. Continuous pressure recordings were begun on 18.5 dpc and continued through parturition and 12 h postpartum (19.5 dpc for wild-type mice) or until 21.5 dpc or signs of labor dystocia required euthanasia of the dam. Pressure measurements were exported every 10 s. Hourly pressure averages (mmHg) were calculated with Dataquest ART 4.2 software (DSI), in which all data points were averaged within the hour. The photocycle of light and dark cycles of the mice were noted for each pregnancy.

Serum Hormone Measurements. Blood was collected from timed pregnant and pseudo pregnant mice through retro-orbital bleeding and allowed to clot in serum separator microtainer tubes (Becton Dickinson) before centrifugation

at 2,000 × *g* for 10 min for serum isolation. Serum levels of estrogen and progesterone were measured by enzyme linked immunosorbent assay and radioimmunoassay, respectively, by the Ligand Assay and Analysis Core at the University of Virginia Center for Research and Reproduction.

Histological Analysis. Transverse sections of the miduterine horn were prepared, processed, and paraffin embedded as described (105). For immunohistochemical analysis, tissue sections were incubated overnight at 4 °C with primary antibodies: Myc (1:500 dilution, Cell Signaling Technology), PGR (1:500 dilution, Santa Cruz Biotechnology, Inc.), and Myh11 (1:200, Santa Cruz Biotechnology, Inc.). Sections were incubated with biotin-labeled secondary antibody of goat anti-rabbit or anti-mouse IgG (Vector Laboratories), followed by incubation with horseradish peroxidase conjugated avidin (Vector Laboratories). The 3, 3′ diaminobenzidine peroxidase substrate kit (Vector Laboratories) was used to visualize immunoreactivity, followed by counterstaining with hematoxylin (Poly Scientific). Images were captured using the Nikon Eclipse Ci-L upright microscope (Nikon Instruments), and digital images were processed and assembled using Adobe Photoshop (version CS5, Adobe Systems).

For immunofluorescence analysis, the following primary antibodies were used: Myh11 (1:200 dilution, Santa Cruz Biotechnology, Inc.), smooth muscle actin (1:400 dilution, Abcam), and EGFP (1:400 dilution, Abcam). Slides were incubated with secondary antibodies conjugated with Alexa Fluor 488 or 594 (Invitrogen) and mounted using ProLong Gold Slowfade media with DAPI (Invitrogen).

Western Blot. Protein from fresh or flash-frozen tissues were extracted by the Ambion PARIS kit (AM1921, Thermo Fisher Scientific) per manufacturer's instruction. Protein from cells were isolated by the radioimmunoprecipitation assay buffer. Primary antibodies used in this study include PGR (1:500 dilution, sc-7208, Santa Cruz Biotechnology), PLCL1 (1:500 dilution, HPA031849, Sigma Life Science), PLCL2 (1:500 dilution, 17421-1-AP, Proteintech), and GAPDH (1:1,000 dilution, 2118S, Cell Signaling).

RNA Extraction. Uterine tissues from the antimesometrial side of implantation sites were isolated, followed by homogenization by the Bead Mill 24 Homogenizer (15-340-163, Fisher Scientific) in Bead Mill Tubes (15-340-154 Fisher Scientific) with 1 mL TRIzol (15596026, Thermo Fisher Scientific). Tissue debris were pelleted and removed by centrifugation at 12,000 × *g* for 10 min at 4 °C. After adding 200 μL 1-Bromo-3-chloropropane, samples were manually shaken for 20 s followed by incubation at room temperature for 3 min. Phase separation was conducted by centrifugation at 12,000 × *g* for 18 min at 4 °C. The RNA-containing aqueous layer was retained and subsequently mixed with 500 μL 200 proof ethanol. The mixture was then passed through the RNA binding column of an RNeasy Mini Kit (74104, Qiagen), followed by washing and the elution steps described in the manufacturer's handbook.

qRT-PCR. Total RNA was quantified using a NanoDrop Spectrophotometer ND-1000 (NanoDrop Technologies) before RNA (2.5 μg) was reverse transcribed to generate complementary DNA (cDNA) using the SuperScript VILO cDNA Synthesis Kit (Life Technologies) or by the Transcriptor First Strand cDNA Synthesis Kit (04379012001, Roche Life Science, Penzberg). Quantitative real-time PCR analysis was performed using the TaqMan Universal Master Mix II (Life Technologies), SsoAdvanced Universal SYBR Green Supermix (1725270, Bio-Rad), or SsoAdvanced Universal Probes Supermix (1725280, Bio-Rad) on the CFX Connect Real-Time PCR Detection System (1855201, Bio-Rad) based on manufacturer's instruction. Ribosomal RNA (rRNA, 18S) was used as an internal control. The 18S rRNA probe is from Thermo Fisher Scientific (4319413E). Primers used in this study include mouse *Plcl2* forward cgctgtgta tgaaaagatcgtg, mouse *Plcl2* reverse gtgcctatgctgtgcaagtg, human *PLCL1* forward caggaaaagattgtacagtgtcaga, human *PLCL1* reverse tttgcccccaaattatgaag, human *PLCL2* forward tatgacatgatgattcagtccctc, human *PLCL2* reverse ttcctt ggtgcctatgctgt, human ACTA2 forward ctgttccagccatccttcat, human ACTA2 reverse tcatgatgctgttgtaggtggt, human TAGLN forward cagtgtggccctgatgtg, and human TAGLN reverse caccagcttgctcagaatca. Probes used include *Pgr* (*Mus musculus*) Mm 00435628_m1, *Trpc3* (*Mus musculus*) Mm00444690_m1, and *Oxtr* (*Mus musculus*) Mm01182684_m1 from Thermo Fisher.

RNA-Seq. The libraries prepared from the extracted RNA samples were sequenced with 43.8 to 83.8 million 76-base-pair (bp) paired-end reads per sample. The raw reads were filtered by removing low quality reads (average quality scores <20), followed by removing adapter-carrying reads using Cutadapt (v2.7) (106). The reads were further cleaned by decontaminating rRNA reads through mapping to the mouse rRNA sequences using Bowtie (v2.2.5) (107). Then, the processed reads were normalized to the same number of reads for aligning to mm10 genome using Spliced Transcripts Alignment to a Reference software version 2.7.0f (108). The number of fragments (read pairs) that mapped to the gene models were counted using the featureCounts (v1.6.4) function available in the software package Subread (109). Differential expression analysis was performed using R package DESeq2 (v1.24.0) (110). Differentially expressed genes were determined using the following combined cutoffs: detected with mean FPKM ≥1 in at least one of the conditions, absolute fold change of ≥1.3, and unadjusted $P < 0.05$. The RNA-Seq data were deposited to the National Center for Biotechnology Information (NCBI) Gene Expression Omnibus repository (GEO accession number GSE146634).

To examine the transgene and overall *Pgr* expression, regions of 25 bp length from the transgene-specific sequence (GTTGTGGATCTGCGATCTAAGTAAG) and PGR-A and PGR-B shared sequence in exon 2 (GCTTAATCTGCGGGGATGAAGCATC) were used for quantification. Among all the raw reads from each sample, we identified the individual reads including each of these 25 bp regions. For direct comparison of expression levels of each target sequence among samples, the final normalized read count was based on the read count per 100 million raw individual reads of each sample.

GO and Pathway Enrichment Analyses. Differentially expressed genes were mined by the BaseSpace Correlation Engine (Illumina) for GO Terms and MSigDB and IPA (Qiagen) for enrichment of molecular activities and diseases and functions.

Gene Signature Analysis. The publicly available human microarray datasets GSE137551 and GSE32178 were scored for manifestation of the mouse model-derived PGR-A and PGR-B gene signatures using the published t-score metric (111, 112). A gene signature score, t-score, was calculated for each external profile with the two-sided t-statistic test, within the profile, comparing between the group of the PGR isoform induced genes with the group of the PGR isoform repressed genes. In this way, the t-score contrasted the patterns of the "PGR isoform induced" genes against those of the "PGR isoform repressed" genes and could be used to derive a single value denoting coordinate expression of the two gene sets. A score greater than zero indicates a positive correlation with the mouse PGR gene signature and vice versa. Within each human dataset, where multiple probes referred to the same gene, the probes with the highest variation were taken to represent the gene; genes were then centered to SDs from the median across sample profiles.

Generation of PLCL1 and PLCL2 Overexpression Cells by CRISPRa. hTERT-HM cells (58) were transduced with IGI-P0492 pHR-dCas9-NLS-VPR-mCherry (a gift from Jacob Corn; Addgene plasmid #102245; http://n2t.net/addgene:102245; Research Resource Identifier: Addgene_102245) and guide RNA (gRNA)-blue fluorescent protein (BFP)–expressing vectors. gRNA-BFP–expressing vectors were synthesized with the guide sequences TCGAGTACATTAGCCCCGCT and GCGCGCGTGTGCAAACCCGG for PLCL1, GCGCACGGTTAAAGTCGCGG and GCGCCAAAAATAACCCGCGC for PLCL2, and GCACTACCAGAGCTAACTCA for scrambled control (VectorBuilder, catalog #VB200730-1266nkh, VB200730-1270edv, and VB200731-1090zyk, respectively). Cells positive for both GFP and BFP were enriched by three rounds of cell sorting and expansion cycles to select the stable expression pools. Cells were maintained in the Dulbecco's modified Eagle medium (DMEM)/F12 medium (Thermo Fisher 11330032) with 10% fetal bovine serum (Thermo Fisher 10437028) and 1× antibiotic–antimycotic (Thermo Fisher 15240062) as described previously (58).

Collagen Contractility Assay. The cell contraction assay was performed on bovine type 1 collagen and the 48-well cell contraction plate (floating model) per manufacturer's instruction manual (Cell Biolabs, Inc. CBA-5021) with 105,000 cells/well. After collagen polymerization, cells were cultured in DMEM/F12 medium (Thermo Fisher 11330032), 10% fetal bovine serum (Thermo Fisher 10437028), 1× antibiotic–antimycotic (Thermo Fisher 15240062), and 200 nM oxytocin (Sigma O4375) (113) for 2 d. Images of collagen gels were taken using a ZEISS Axiocam ERc 5s under a Leica MZ12 Microscope with a ruler (Fine Science Tools). Each collagen gel had its diameter measured twice at a perpendicular angle, and the number in average was reported.

Statistical Analysis. Statistical analysis was performed with the R Commander package (RStudio, Inc.) or GraphPad Prism 8 (GraphPad Software) unless specified otherwise. Data are presented as the mean ± SEM. *P* values less than 0.05 were defined as statistically significant.

Data Availability. RNA-Seq data have been deposited in the NCBI Gene Expression Omnibus (GSE146634).

ACKNOWLEDGMENTS. We thank the National Institute of Environmental Health Sciences (NIEHS) Epigenomic and DNA Sequencing Core, the Viral Vector Core, the Integrative Bioinformatics Supportive Group, the Knockout Mouse Core, and the Comparative Medicine Branch at the NIEHS, as well as the Research in Reproduction Ligand Assay and Analysis Core, University of Virginia for technical support. We also thank Dr. Corey Reynolds for telemetry and ultrasound assistance and Mr. Linwood Koonce for mouse colony management. This work was supported by an Intramural Research Program of the NIEHS, NIH project nos. Z1AES103311 (F.J.D.) and Z99-ES999999 (S.-P.W.), as well as an NIH extramural research program of the National Institute of Child Health and Human Development grant no. RO1 HD042311 (J.P.L.). O.M.E. is supported by the NIEHS Postbaccalaureate Intramural Research Training Award. This work is supported in part by the Burroughs Wellcome Fund and March of Dimes.

1. S. Govindappagari, N. Greene, R. Burwick, M. S. Wong, K. D. Gregory, Maternal and neonatal morbidity after 4 and 6 hours of protracted active labor in nulliparous term pregnancies. *Obstet. Gynecol.* **135**, 185–193 (2020).
2. Y. Zipori, O. Grunwald, Y. Ginsberg, R. Beloosesky, Z. Weiner, The impact of extending the second stage of labor to prevent primary cesarean delivery on maternal and neonatal outcomes. *Am. J. Obstet. Gynecol.* **220**, 191.e191–191.e197 (2019).
3. H. Blencowe *et al*.; Born Too Soon Preterm Birth Action Group, Born too soon: The global epidemiology of 15 million preterm births. *Reprod. Health* **10** (suppl. 1), S2 (2013).
4. H. A. Frey, M. A. Klebanoff, The epidemiology, etiology, and costs of preterm birth. *Semin. Fetal Neonatal Med.* **21**, 68–73 (2016).
5. M. S. Harrison, R. L. Goldenberg, Global burden of prematurity. *Semin. Fetal Neonatal Med.* **21**, 74–79 (2016).
6. J. A. Martin, M. J. Osterman, P. D. Sutton, Are preterm births on the decline in the United States? Recent data from the national vital statistics system. *NCHS Data Brief*, 1–8 (2010).
7. C. E. Ransom, A. P. Murtha, Progesterone for preterm birth prevention. *Obstet. Gynecol. Clin. North Am.* **39**, 1–16, vii (2012).
8. R. Romero, L. Yeo, P. Chaemsaithong, T. Chaiworapongsa, S. S. Hassan, Progesterone to prevent spontaneous preterm birth. *Semin. Fetal Neonatal Med.* **19**, 15–26 (2014).
9. P. J. Meis *et al*.; National Institute of Child Health and Human Development Maternal-Fetal Medicine Units Network, Prevention of recurrent preterm delivery by 17 alpha-hydroxyprogesterone caproate. *N. Engl. J. Med.* **348**, 2379–2385 (2003).
10. S. Mesiano, Myometrial progesterone responsiveness and the control of human parturition. *J. Soc. Gynecol. Investig.* **11**, 193–202 (2004).
11. T. Zakar, F. Hertelendy, Progesterone withdrawal: Key to parturition. *Am. J. Obstet. Gynecol.* **196**, 289–296 (2007).
12. T. Zakar, S. Mesiano, How does progesterone relax the uterus in pregnancy? *N. Engl. J. Med.* **364**, 972–973 (2011).
13. S. G. Matthews, W. Gibb, S. J. Lye, S. J. Lye; Challis JRG, Endocrine and paracrine regulation of birth at term and preterm. *Endocr. Rev.* **21**, 514–550 (2000).
14. B. F. Mitchell, M. J. Taggart, Are animal models relevant to key aspects of human parturition? *Am. J. Physiol. Regul. Integr. Comp. Physiol.* **297**, R525–R545 (2009).
15. J. M. Bassett, T. J. Oxborrow, I. D. Smith, G. D. Thorburn, The concentration of progesterone in the peripheral plasma of the pregnant Ewe. *J. Endocrinol.* **45**, 449–457 (1969).
16. R. K. Bartholomeusz, N. W. Bruce, C. E. Martin, P. E. Hartmann, Serial measurement of arterial plasma progesterone levels throughout gestation and parturition in individual rats. *Acta Endocrinol. (Copenh.)* **82**, 436–443 (1976).
17. L. A. Vodstrcil *et al*., Progesterone withdrawal, and not increased circulating relaxin, mediates the decrease in myometrial relaxin receptor (RXFP1) expression in late gestation in rats. *Biol. Reprod.* **83**, 825–832 (2010).
18. B. B. Virgo, G. D. Bellward, Serum progesterone levels in the pregnant and postpartum laboratory mouse. *Endocrinology* **95**, 1486–1490 (1974).
19. S. W. Walsh, F. Z. Stanczyk, M. J. Novy, Daily hormonal changes in the maternal, fetal, and amniotic fluid compartments before parturition in a primate species. *J. Clin. Endocrinol. Metab.* **58**, 629–639 (1984).
20. D. Tulchinsky, C. J. Hobel, E. Yeager, J. R. Marshall, Plama estradiol, estriol, and progesterone in human pregnancy. II. Clinical applications in Rh-isoimmunization disease. *Am. J. Obstet. Gynecol.* **113**, 766–770 (1972).
21. R. S. Boroditsky, F. I. Reyes, J. S. Winter, C. Faiman, Maternal serum estrogen and progesterone concentrations preceding normal labor. *Obstet. Gynecol.* **51**, 686–691 (1978).
22. P. R. Lewis, P. M. Galvin, R. V. Short, Salivary oestriol and progesterone concentrations in women during late pregnancy, parturition and the puerperium. *J. Endocrinol.* **115**, 177–181 (1987).
23. C. E. Rubens *et al*., Prevention of preterm birth: Harnessing science to address the global epidemic. *Sci. Transl. Med.* **6**, 262sr5 (2014).
24. E. M. Lackritz *et al*.; Preterm Birth Research Priority Setting Group, A solution pathway for preterm birth: Accelerating a priority research agenda. *Lancet Glob. Health* **1**, e328–e330 (2013).
25. J. A. Keelan, M. Coleman, M. D. Mitchell, The molecular mechanisms of term and preterm labor: Recent progress and clinical implications. *Clin. Obstet. Gynecol.* **40**, 460–478 (1997).
26. A. Csapo, Progesterone block. *Am. J. Anat.* **98**, 273–291 (1956).
27. A. I. Csapo, W. G. Wiest, An examination of the quantitative relationship between progesterone and the maintenance of pregnancy. *Endocrinology* **85**, 735–746 (1969).
28. A. G. Brown, R. S. Leite, J. F. Strauss III, Mechanisms underlying "functional" progesterone withdrawal at parturition. *Ann. N. Y. Acad. Sci.* **1034**, 36–49 (2004).
29. S. Mesiano, T. N. Welsh, Steroid hormone control of myometrial contractility and parturition. *Semin. Cell Dev. Biol.* **18**, 321–331 (2007).
30. L. Nadeem *et al*., Molecular evidence of functional progesterone withdrawal in human myometrium. *Nat. Commun.* **7**, 11565 (2016).
31. B. Patel *et al*., Role of nuclear progesterone receptor isoforms in uterine pathophysiology. *Hum. Reprod. Update* **21**, 155–173 (2015).
32. M. A. Bedaiwy *et al*., Abundance and localization of progesterone receptor isoforms in endometrium in women with and without endometriosis and in peritoneal and ovarian endometriotic implants. *Reprod. Sci.* **22**, 1153–1161 (2015).
33. A. A. Mills *et al*., Characterization of progesterone receptor isoform expression in fetal membranes. *Am. J. Obstet. Gynecol.* **195**, 998–1003 (2006).
34. B. Mulac-Jericevic, R. A. Mullinax, F. J. DeMayo, J. P. Lydon, O. M. Conneely, Subgroup of reproductive functions of progesterone mediated by progesterone receptor-B isoform. *Science* **289**, 1751–1754 (2000).
35. O. M. Conneely, B. Mulac-Jericevic, J. P. Lydon, F. J. De Mayo, Reproductive functions of the progesterone receptor isoforms: Lessons from knock-out mice. *Mol. Cell. Endocrinol.* **179**, 97–103 (2001).
36. O. M. Conneely, B. Mulac-Jericevic, J. P. Lydon, Progesterone-dependent regulation of female reproductive activity by two distinct progesterone receptor isoforms. *Steroids* **68**, 771–778 (2003).
37. A. A. Merlino *et al*., Nuclear progesterone receptors in the human pregnancy myometrium: Evidence that parturition involves functional progesterone withdrawal mediated by increased expression of progesterone receptor-A. *J. Clin. Endocrinol. Metab.* **92**, 1927–1933 (2007).
38. D. X. Wen, Y. F. Xu, D. E. Mais, M. E. Goldman, D. P. McDonnell, The A and B isoforms of the human progesterone receptor operate through distinct signaling pathways within target cells. *Mol. Cell Biol.* **14**, 8356–8364 (1994).
39. D. P. McDonnell, M. M. Shahbaz, E. Vegeto, M. E. Goldman, The human progesterone receptor A-form functions as a transcriptional modulator of mineralocorticoid receptor transcriptional activity. *J. Steroid Biochem. Mol. Biol.* **48**, 425–432 (1994).
40. E. Vegeto *et al*., Human progesterone receptor A form is a cell- and promoter-specific repressor of human progesterone receptor B function. *Mol. Endocrinol.* **7**, 1244–1255 (1993).
41. H. How *et al*., Myometrial estradiol and progesterone receptor changes in preterm and term pregnancies. *Obstet. Gynecol.* **86**, 936–940 (1995).
42. H. Tan, L. Yi, N. S. Rote, W. W. Hurd, S. Mesiano, Progesterone receptor-A and -B have opposite effects on proinflammatory gene expression in human myometrial cells: Implications for progesterone actions in human pregnancy and parturition. *J. Clin. Endocrinol. Metab.* **97**, E719–E730 (2012).
43. D. B. Hardy, B. A. Janowski, D. R. Corey, C. R. Mendelson, Progesterone receptor plays a major antiinflammatory role in human myometrial cells by antagonism of nuclear factor-kappaB activation of cyclooxygenase 2 expression. *Mol. Endocrinol.* **20**, 2724–2733 (2006).
44. H. N. Jabbour, R. W. Kelly, H. M. Fraser, H. O. Critchley, Endocrine regulation of menstruation. *Endocr. Rev.* **27**, 17–46 (2006).
45. W. Ke *et al*., Histone deacetylase 1 regulates the expression of progesterone receptor A during human parturition by occupying the progesterone receptor A promoter. *Reprod. Sci.* **23**, 955–964 (2016).
46. K. Lei *et al*., Progesterone and the repression of myometrial inflammation: The roles of MKP-1 and the AP-1 system. *Mol. Endocrinol.* **29**, 1454–1467 (2015).
47. Z. Zeng, M. C. Velarde, F. A. Simmen, R. C. Simmen, Delayed parturition and altered myometrial progesterone receptor isoform A expression in mice null for Krüppel-like factor 9. *Biol. Reprod.* **78**, 1029–1037 (2008).
48. S. Y. Chai, R. Smith, T. Zakar, C. Mitchell, G. Madsen, Term myometrium is characterized by increased activating epigenetic modifications at the progesterone receptor-A promoter. *Mol. Hum. Reprod.* **18**, 401–409 (2012).
49. S. Mesiano *et al*., Progesterone withdrawal and estrogen activation in human parturition are coordinated by progesterone receptor A expression in the myometrium. *J. Clin. Endocrinol. Metab.* **87**, 2924–2930 (2002).
50. G. J. Haluska *et al*., Progesterone receptor localization and isoforms in myometrium, decidua, and fetal membranes from rhesus macaques: Evidence for functional progesterone withdrawal at parturition. *J. Soc. Gynecol. Investig.* **9**, 125–136 (2002).
51. S. Y. Oh *et al*., Progesterone receptor isoform (A/B) ratio of human fetal membranes increases during term parturition. *Am. J. Obstet. Gynecol.* **193**, 1156–1160 (2005).
52. S. Goldman, A. Weiss, I. Almalah, E. Shalev, Progesterone receptor expression in human decidua and fetal membranes before and after contractions: Possible mechanism for functional progesterone withdrawal. *Mol. Hum. Reprod.* **11**, 269–277 (2005).
53. A. R. Fuchs, F. Fuchs, P. Husslein, M. S. Soloff, Oxytocin receptors in the human uterus during pregnancy and parturition. *Am. J. Obstet. Gynecol.* **150**, 734–741 (1984).
54. M. S. Soloff, D. L. Cook Jr, Y. J. Jeng, G. D. Anderson, In situ analysis of interleukin-1-induced transcription of cox-2 and il-8 in cultured human myometrial cells. *Endocrinology* **145**, 1248–1254 (2004).
55. J. L. Cook, M. C. Shallow, D. B. Zaragoza, K. I. Anderson, D. M. Olson, Mouse placental prostaglandins are associated with uterine activation and the timing of birth. *Biol. Reprod.* **68**, 579–587 (2003).
56. D. M. Olson, The role of prostaglandins in the initiation of parturition. *Best Pract. Res. Clin. Obstet. Gynaecol.* **17**, 717–730 (2003).
57. J. M. Pabona, D. Zhang, D. S. Ginsburg, F. A. Simmen, R. C. Simmen, Prolonged pregnancy in women is associated with attenuated myometrial expression of progesterone receptor co-regulator Krüppel-like Factor 9. *J. Clin. Endocrinol. Metab.* **100**, 166–174 (2015).

58. J. Condon *et al*., Telomerase immortalization of human myometrial cells. *Biol. Reprod.* **67**, 506–514 (2002).
59. G. A. Peters *et al*., Inflammatory stimuli increase progesterone receptor-A stability and transrepressive activity in myometrial cells. *Endocrinology*, 20161537 (2016).
60. P. Amini *et al*., Human parturition involves phosphorylation of progesterone receptor-A at serine-345 in myometrial cells. *Endocrinology* **157**, 4434–4445 (2016).
61. S. Mesiano, Y. Wang, E. R. Norwitz, Progesterone receptors in the human pregnancy uterus: Do they hold the key to birth timing? *Reprod. Sci.* **18**, 6–19 (2011).
62. N. E. Renthal *et al*., Molecular regulation of parturition: A myometrial perspective. *Cold Spring Harb. Perspect. Med.* **5**, a023069 (2015).
63. H. B. Xin, K. Y. Deng, M. Rishniw, G. Ji, M. I. Kotlikoff, Smooth muscle expression of Cre recombinase and eGFP in transgenic mice. *Physiol. Genomics* **10**, 211–215 (2002).
64. M. Wetendorf *et al*., Decreased epithelial progesterone receptor A at the window of receptivity is required for preparation of the endometrium for embryo attachment. *Biol. Reprod.* **96**, 313–326 (2017).
65. L. Hai *et al*., A mouse model engineered to conditionally express the progesterone receptor-B isoform. *Genesis* **56**, e23223 (2018).
66. N. Salomonis *et al*., Alternative splicing regulates mouse embryonic stem cell pluripotency and differentiation. *Proc. Natl. Acad. Sci. U.S.A.* **107**, 10514–10519 (2010).
67. A. Liberzon, A description of the molecular signatures database (MSigDB) web site. *Methods Mol. Biol.* **1150**, 153–160 (2014).
68. M. Wetendorf *et al*., Constitutive expression of progesterone receptor isoforms promotes the development of hormone-dependent ovarian neoplasms. *Sci. Signal.* **13**, eaaz9646 (2020).
69. S. Arrowsmith, S. Wray, Oxytocin: Its mechanism of action and receptor signalling in the myometrium. *J. Neuroendocrinol.* **26**, 356–369 (2014).
70. P. Balakumar, G. Jagadeesh, A century old renin-angiotensin system still grows with endless possibilities: AT1 receptor signaling cascades in cardiovascular physiopathology. *Cell. Signal.* **26**, 2147–2160 (2014).
71. C. Jing *et al*., TRPC3 overexpression promotes the progression of inflammation-induced preterm labor and inhibits T cell activation. *Cell. Physiol. Biochem.* **45**, 378–388 (2018).
72. E. Dallot *et al*., Contraction of cultured human uterine smooth muscle cells after stimulation with endothelin-1. *Biol. Reprod.* **68**, 937–942 (2003).
73. M. Adli, The CRISPR tool kit for genome editing and beyond. *Nat. Commun.* **9**, 1911 (2018).
74. T. Hofmann *et al*., Direct activation of human TRPC6 and TRPC3 channels by diacylglycerol. *Nature* **397**, 259–263 (1999).
75. J. Qin *et al*., COUP-TFII inhibits TGF-β-induced growth barrier to promote prostate tumorigenesis. *Nature* **493**, 236–240 (2013).
76. S. P. Wu *et al*., Dynamic transcriptome, accessible genome, and PGR cistrome profiles in the human myometrium. *FASEB J.* **34**, 2252–2268 (2020).
77. A. Merlino *et al*., Nuclear progesterone receptor expression in the human fetal membranes and decidua at term before and after labor. *Reprod. Sci.* **16**, 357–363 (2009).
78. O. M. Conneely, J. P. Lydon, F. De Mayo, B. W. O'Malley, Reproductive functions of the progesterone receptor. *J. Soc. Gynecol. Investig.* **7**(1, suppl.)S25–S32 (2000).
79. C. P. Regan, I. Manabe, G. K. Owens, Development of a smooth muscle-targeted cre recombinase mouse reveals novel insights regarding smooth muscle myosin heavy chain promoter regulation. *Circ. Res.* **87**, 363–369 (2000).
80. H. Wang *et al*., Aberrant cannabinoid signaling impairs oviductal transport of embryos. *Nat. Med.* **10**, 1074–1080 (2004).
81. R. A. Chi *et al*., WNK1 regulates uterine homeostasis and its ability to support pregnancy. *JCI Insight* **5**, 141832 (2020).
82. E. D. Albrecht, G. J. Pepe, Regulation of uterine spiral artery remodeling: A review. *Reprod. Sci.* **27**, 1932–1942 (2020).
83. S. D. Harding *et al*., The GUDMAP database–An online resource for genitourinary research. *Development* **138**, 2845–2853 (2011).
84. H.-R. Kim *et al*., Estrogen induces EGR1 to fine-tune its actions on uterine epithelium by controlling PR signaling for successful embryo implantation. *FASEB J.* **32**, 1184–1195 (2018).
85. R. Migale *et al*., Specific lipopolysaccharide serotypes induce differential maternal and neonatal inflammatory responses in a murine model of preterm labor. *Am. J. Pathol.* **185**, 2390–2401 (2015).
86. M. Molnár, J. Rigó Jr, R. Romero, F. Hertelendy, Oxytocin activates mitogen-activated protein kinase and up-regulates cyclooxygenase-2 and prostaglandin production in human myometrial cells. *Am. J. Obstet. Gynecol.* **181**, 42–49 (1999).
87. O. Shynlova, P. Tsui, A. Dorogin, B. L. Langille, S. J. Lye, The expression of transforming growth factor beta in pregnant rat myometrium is hormone and stretch dependent. *Reproduction* **134**, 503–511 (2007).
88. N. K. Kuşcu *et al*., Immunolocalization of transforming growth factor-beta 3 in pregnant human myometrium. *Acta Obstet. Gynecol. Scand.* **80**, 1079–1083 (2001).
89. P. Hatthachote, J. Morgan, W. Dunlop, G. N. Europe-Finner, J. I. Gillespie, Gestational changes in the levels of transforming growth factor-beta1 (TGFbeta1) and TGFbeta receptor types I and II in the human myometrium. *J. Clin. Endocrinol. Metab.* **83**, 2987–2992 (1998).
90. S. Kunzmann, B. Ottensmeier, C. P. Speer, M. Fehrholz, Effect of progesterone on Smad signaling and TGF-β/Smad-regulated genes in lung epithelial cells. *PLoS One* **13**, e0200661 (2018).
91. J. Lecanda *et al*., Transforming growth factor-beta, estrogen, and progesterone converge on the regulation of p27Kip1 in the normal and malignant endometrium. *Cancer Res.* **67**, 1007–1018 (2007).
92. M. Otsuki, K. Fukami, T. Kohno, J. Yokota, T. Takenawa, Identification and characterization of a new phospholipase C-like protein, PLC-L(2). *Biochem. Biophys. Res. Commun.* **266**, 97–103 (1999).
93. T. Kanematsu, H. Takeuchi, M. Terunuma, M. Hirata, PRIP, a novel Ins(1,4,5)P3 binding protein, functional significance in Ca2+ signaling and extension to neuroscience and beyond. *Mol. Cells* **20**, 305–314 (2005).
94. J. Muter *et al*., Progesterone-dependent induction of phospholipase C-related catalytically inactive protein 1 (PRIP-1) in decidualizing human endometrial stromal cells. *Endocrinology* **157**, 2883–2893 (2016).
95. K. Takenaka *et al*., Role of phospholipase C-L2, a novel phospholipase C-like protein that lacks lipase activity, in B-cell receptor signaling. *Mol. Cell Biol.* **23**, 7329–7338 (2003).
96. S. Asano *et al*., Suppression of cell migration by phospholipase C-related catalytically inactive protein-dependent modulation of PI3K signalling. *Sci. Rep.* **7**, 5408 (2017).
97. A. Murakami, M. Matsuda, Y. Harada, M. Hirata, Phospholipase C-related, but catalytically inactive protein (PRIP) up-regulates osteoclast differentiation via calcium-calcineurin-NFATc1 signaling. *J. Biol. Chem.* **292**, 7994–8006 (2017).
98. K. Oue *et al*., Phospholipase C-related catalytically inactive protein is a new modulator of thermogenesis promoted by β-Adrenergic receptors in Brown adipocytes. *J. Biol. Chem.* **291**, 4185–4196 (2016).
99. M. Matsuda *et al*., Involvement of phospholipase C-related inactive protein in the mouse reproductive system through the regulation of gonadotropin levels. *Biol. Reprod.* **81**, 681–689 (2009).
100. P. Brighton, A. Blanks, "Control of uterine contractions." US Patent 2016/O161487 A1 (2016).
101. National Research Council, *Guide for the Care and Use of Laboratory Animals* (National Academies Press, Washington, DC, 8th Ed., 2011).
102. M. C. Peavey *et al*., A novel use of three-dimensional high-frequency ultrasonography for early pregnancy characterization in the mouse. *J. Vis. Exp.*, e56207 (2017).
103. S. L. Pierce, W. Kutschke, R. Cabeza, S. K. England, In vivo measurement of intrauterine pressure by telemetry: A new approach for studying parturition in mouse models. *Physiol. Genomics* **42**, 310–316 (2010).
104. C. C. Rada, S. L. Pierce, C. A. Grotegut, S. K. England, Intrauterine telemetry to measure mouse contractile pressure in vivo. *J. Vis. Exp.*, e52541 (2015).
105. M. J. Large *et al*., The epidermal growth factor receptor critically regulates endometrial function during early pregnancy. *PLoS Genet.* **10**, e1004451 (2014).
106. M. Martin Cutadapt removes adapter sequences from high-throughput sequencing reads. *EMBnet.J* **17**, 10–12 (2011).
107. B. Langmead, S. L. Salzberg, Fast gapped-read alignment with Bowtie 2. *Nat. Methods* **9**, 357–359 (2012).
108. A. Dobin *et al*., STAR: Ultrafast universal RNA-seq aligner. *Bioinformatics* **29**, 15–21 (2013).
109. Y. Liao, G. K. Smyth, W. Shi, featureCounts: an efficient general purpose program for assigning sequence reads to genomic features. *Bioinformatics* **30**, 923–930 (2014).
110. M. I. Love, W. Huber, S. Anders, Moderated estimation of fold change and dispersion for RNA-seq data with DESeq2. *Genome Biol.* **15**, 550 (2014).
111. C. J. Creighton *et al*., Insulin-like growth factor-I activates gene transcription programs strongly associated with poor breast cancer prognosis. *J. Clin. Oncol.* **26**, 4078–4085 (2008).
112. S. P. Wu *et al*., Increased COUP-TFII expression in adult hearts induces mitochondrial dysfunction resulting in heart failure. *Nat. Commun.* **6**, 8245 (2015).
113. J. J. Ferreira *et al*., Oxytocin can regulate myometrial smooth muscle excitability by inhibiting the Na^+ -activated K^+ channel, Slo2.1. *J. Physiol.* **597**, 137–149 (2019).